BENCHMARK OF LIVE EXPERIMENTS WITH MAAP5.04 ALPHA

B. Ozar, S. J. Lee, M. Epstein* and C. Y. Paik
Fauske & Associates, LLC
16W070 83rd St., Burr Ridge, IL 60527, USA
ozar@fauske.com; lee@fauske.com; michaelepstein@aol.com; paik@fauske.com

ABSTRACT

The lower plenum models related to molten pool behavior and crust formation in MAAP*5.04 Alpha are benchmarked against the LIVE-L1 and LIVE-L3 test results. The experimental test facility and procedures are described and the key measured quantities are explained in detail. MAAP4 and earlier versions of MAAP5 have considered a single continuous debris pool and tracked the mass, energy and composition of the entire pool. However, a new feature, multi-layer model, is added to MAAP5.04 Alpha. Multi-layer debris model axially nodalizes the debris pool and tracks the mass, composition and energy of each individual layer separately. The MAAP 5.04 Alpha code shows reasonably good agreement with the experimental data both for LIVE-L1 and LIVE-L3 tests. Particularly, the multi –layer debris model is able to predict the temperature distribution within the debris pool reasonably well. The non-prototypic melt pool (no top crust) and discrete heating arrays are identified as important factors affecting the benchmarking.

*The MAAP code is owned by the Electric Power Research Institute (EPRI), and was developed and is maintained by Fauske and Associates, LLC.

KEYWORDS
MAAP, severe accident, lower plenum, debris bed

1. INTRODUCTION

During a severe accident in a nuclear power plant, a considerable amount of core material may be relocated into the reactor pressure vessel (RPV) lower head, similar to the core relocation that took place in the TMI-2 accident. This core relocation can impose considerable thermal loads on the lower head structure. Modeling the behavior of a corium pool in the lower head is important in assessing accident mitigation strategies, especially in the evaluation of in-vessel melt retention by external vessel cooling. The behavior of the corium pool in the lower head is complicated by timing and other intervening or concurrent phenomena which are occurring during a severe accident.

Since the TMI-2 accident, continuous research activities have been focused on gaining a better understanding of the core melt progression that is expected to occur in the RPV lower head, and of the related phenomenological uncertainties. The COPO [1] experimental facility was a two-dimensional slice of the one-half scale lower portion of the reactor vessel at the Loviisa nuclear plant in Finland. The oxidic pool was simulated by $ZnSO_4$-H_2O solution and heated volumetrically by Joule heating. Heat fluxes were measured under isothermal boundary conditions. The BALI [2] experimental facility was a

* Retired from Fauske and Associates, LLC.

two-dimensional slice of the full scale French pressurized water reactor (PWR) lower head. The corium melt was simulated by salt water. The ACOPO [3] facility was a one-half scale AP600 lower head test apparatus. Volumetric heating was not used in this experiment. The fluid (water or Freon) was preheated to a high initial temperature and then poured into the vessel. The high bulk to wall temperature differences of up to ~100° C were the unique feature of the ACOPO experiments that was not present in other experiments where the temperature range was rather small. One of the more recent experimental programs is the LIVE [4] tests. LIVE tests were designed to investigate the core melt behavior in the lower plenum of the reactor pressure vessel and the influence of the cooling of the vessel outer surface with water in the conditions that may occur during the meltdown accident of PWRs. To simulate the corium melt, a non-eutectic binary mixture of $NaNO_3$ and KNO_3 was used.

In recent years, there has been a significant increase in the ability to understand and model severe accident phenomena. The results of these increased modeling capabilities provide plant specific insights into what occurs during a severe accident. The MELCOR [5], SCDAP/RELAP5 [6] ASTEC [7], and MAAP5 [8] codes have been widely used by the nuclear industry in modeling severe accidents.

The purpose of this work is to benchmark the models that describe the molten pool behavior in MAAP5.04 Alpha against the LIVE test results. Key parameters such as pool temperatures, downward heat fluxes in the molten pool, crust thicknesses and crust temperatures are compared against the experimental data to validate the MAAP lower plenum model.

2. LIVE-L1 AND LIVE-L3 TESTS

The LIVE test facility was a 1:5 scaled reactor pressure vessel of a typical pressurized water reactor (Figure 1). The inner diameter of the test vessel was 1 m and the wall thickness was 25 mm. The test vessel was made of stainless steel.

To investigate both the transient and steady state behavior of the simulated corium melt, the test vessel was extensively instrumented. Thermocouples were placed inside the vessel to measure the temperature of the melt. In addition, thermocouples were placed on inner and outer vessel wall surfaces. Instrumented plugs were installed on the vessel wall at different positions along 4 meridians at 0 ^{o}, 90 ^{o}, 180 ^{o} and 270 ^{o}. Each plug consisted of a heat flux sensor and 5 thermocouples. The thermocouples were protruding into the melt at different distances from the vessel wall (0, 5, 10, 15, 20 mm). The heat flux sensors were part of the vessel wall and were positioned 1 mm below the inner surface of the test vessel. These sensors measured the heat flux and the corresponding temperature. However, the authors of the test report concluded that the heat flux measurements by these sensors were not reliable [9]. Instead, they recommended using the heat flux measurements obtained from the thermocouples, which were placed on both sides of the vessel wall.

To investigate the effect of external cooling, the test vessel was encased in a second vessel and coolant was circulated in the gap. The coolant was injected at the bottom and was removed at the top.

A heater grid with several independent heating elements was constructed to simulate the decay heat in the molten pool. The heating elements consist of shrouded electrical resistance wires. To uniformly heat the melt pool, six heating planes were installed at 45 mm apart. Each heating plane consisted of a spiral heating coil with a 40 mm gap between each winding. The heating elements were located in a special cage to ensure correct positioning. The heating planes provided a total maximum power of about 28 kW. Heat output in each plane could be controlled individually to facilitate homogeneous heating of the molten pool.

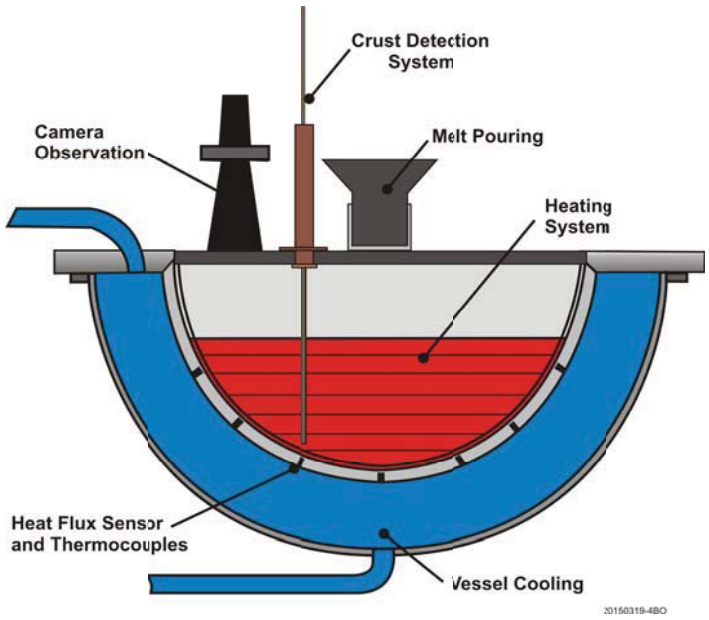

Figure 1. Schematic of Test Apparatus (regenerated based on Fluhrer et al. [9]).

Decay power input into the melt was recorded and melt samples were extracted during the tests. Different openings in the upper lid of the test vessel allowed pouring of the melt to the central region or close to the perimeter of the lower head. At the end of the test, the remaining melt in the vessel was extracted to measure the thickness of the crust formed on the vessel bottom.

Key measurements and their locations are summarized below:

- Pool temperatures: There were multiple thermocouples located inside the test apparatus to measure the temperature of the molten pool. They were located at various elevations (70 mm, 170 mm and 270 mm from the bottom of the vessel) and radial locations (74 mm, 174 mm, 274 mm and 374 mm from the centerline).
- Vessel inner surface temperatures: The vessel inner surface temperatures were measured at various angles. It was measured at 0°, 30°, 51°, 65.5° and 76.5°.
- Vessel outer surface temperatures: The vessel outer surface temperatures were measured at various angles. It was measured at 0°, 30°, 51°, 65.5° and 76.5°.
- Heat fluxes on the vessel wall: The heat flux on the vessel wall was measured at various angles. It was measured at 0°, 30°, 51°, 65.5° and 76.5°.
- Total heat loss on the top of molten pool: The total heat transfer rate to the side and bottom of the molten pool is determined from the heat flux measurements along the vessel wall. The heat removal rate on the top of the molten pool is estimated by subtracting the downward (i.e. to the vessel wall) heat transfer rate from the total heat input.
- Crust temperatures: The crust temperatures were measured using thermocouples that were placed at various distances from the vessel inner surface.
- Crust growth velocity: The crust growth velocity is calculated by using the thermocouple measurements at various distances from the inner surface. The distances between thermocouples and the timing when the freezing front reaches individual thermocouples are used to determine the crust growth velocity.

- Final crust thickness: The final thickness of the crust was measured after the molten mixture was removed from the test apparatus at the end of the test.

To simulate the corium melt a binary mixture of 20 mole percent sodium nitrate ($NaNO_3$) and 80 mole percent potassium nitrate (KNO_3) was used. The mixture has a liquidus temperature of 295°C and a solidus temperature of 235°C (see Figure 2). The physical properties for the 80%/20% KNO_3-$NaNO_3$ binary mixture are summarized in Table 1. The mixture was melted in a separate heating furnace. When the temperature reached about 350°C, 120 liters of the melt was poured into the LIVE test vessel through the pouring spout. The pouring spout was preheated to 350°C. The maximum pouring rate was 7 kg/s.

The LIVE-L1 and LIVE-L3 tests were conducted with same test procedures except that in LIVE-L1 the melt was poured at the center of the vessel whereas, in LIVE-L3, the melt was poured at the side. Table 2 and Table 3 summarize the test parameters and test phases for both tests.

The key information that was gained from the LIVE tests is as follows:

- Unlike the prototypic corium pool, which has uniform temperature boundary conditions, the molten pool in LIVE experiments exhibited no upper crust; the insulated lid limited upward heat transfer and only 20% of the heat loss went upward. In the prototypic corium pool about half of the heat loss goes upward and the other half downward. Therefore, the molten pool heat transfer correlations obtained from prototypic corium pool experiments, such as ACOPO correlation, may not be applicable to the LIVE tests.
- The measured molten pool/crust interface temperature was closer to the liquidus temperature, not the solidus temperature. Note that there is about 50^{o}C difference between the solidus and liquidus temperatures of the KNO_3-$NaNO_3$ binary mixture.
- There was no major difference between the results of the two tests.
- Part of the heater was close to the crust and melted the crust. Particularly, the dip that was observed for the crust measurements at the bottom of the LIVE-L3 was due to the bottom array of the heater preventing any crust formation. The same trend was not observed in LIVE-L1 tests. The molten material was not completely extracted at the conclusion of this test and some of the molten material was allowed to freeze at the bottom of the vessel after the LIVE-L1 test.

3. MAAP5 BENCHMARKING

3.1. Benchmarking Mode:

The code feature to run the LIVE L-1 and L-3 benchmarking is added in MAAP 5.04 Alpha. Both tests are identical in the way they are simulated using MAAP5. Integral experiment benchmarks utilize the full MAAP5 code, and therefore, are performed in the same manner as running conventional sequences. However, benchmark runs visit only selected sections of the code during the execution.

Furthermore, benchmarks generally require prescription of benchmark-specific boundary conditions in addition to those conventionally provided by the MAAP5 parameter file. A benchmark-specific routine BLIVEB was written to provide the initial and boundary conditions, and also to call the lower plenum debris bed model and the vessel wall heat sink model to simulate the LIVE experiments.

Table 1. Physical Properties of KNO_3- $NaNO_3$ 80:20 Mol%

Nitrate $NaNO_3$-KNO_3 20:80 Mol%			
Properties	Temperature, °C		
	300	350	400
c_p [J/kgK]	1369	1369	1369
ρ [kg/m^3]	1897.777	1862.758	1827.739
μ [Pa-s]	3.323E-03	2.508E-03	1.957E-03
ν [m^2/s]	1.75E-06	1.35E-06	1.07E-06
k [W/mK]	0.439	0.422	0.422
β [1/K]	3.81E-04	3.81E-04	3.81E-04
α [m^2/s]	1.69E-07	1.65E-07	1.69E-07
Pr	10.36	8.14	6.35

Table 2. Test Parameters and Test Phase for LIVE-L1

Phase 1: Homogeneous Heat Generation	
Start Time	131 s
Boundary Conditions	Air
Heating Power	18 kW at the Beginning, Stepwise Reduction to 10 kW
Phase 2: Start of Outer Vessel Wall Cooling	
Start Time	7214 s
Boundary Conditions	Water, Continuous Cooling
Cooling Water Flow Rate	~ 0.042 kg/s
Heating Power	10 kW
Phase 3: Reduction of Heat Generation	
Start Time	82,682 s
Boundary Conditions	Water, Continuous Cooling
Cooling Water Flow Rate	~ 0.047 kg/s
Heating Planes	All
Heating Power	7 kW
Heat Generation	Homogeneous[1]
Phase 4: Test Termination and Melt Extraction	
End Time	102,627 s

Table 3. Test Parameters and Test Phase for LIVE-L3

Phase 1: Homogeneous Heat Generation	
Start Time	111 s
Boundary Conditions	Air
Heating Power	18 kW at the Beginning, Stepwise Reduction to 10 kW
Phase 2: Start of Outer Vessel Wall Cooling	
Start Time	7199 s
Boundary Conditions	Water, Continuous Cooling
Cooling Water Flow Rate	~ 0.047 kg/s
Heating Power	10 kW
Phase 3: Reduction of Heat Generation	
Start Time	83,100 s
Boundary Conditions	Water, Continuous Cooling
Cooling Water Flow Rate	~ 0.047 kg/s
Heating Power	7 kW
Phase 4: Test Termination and Melt Extraction	
End Time	102,900 s

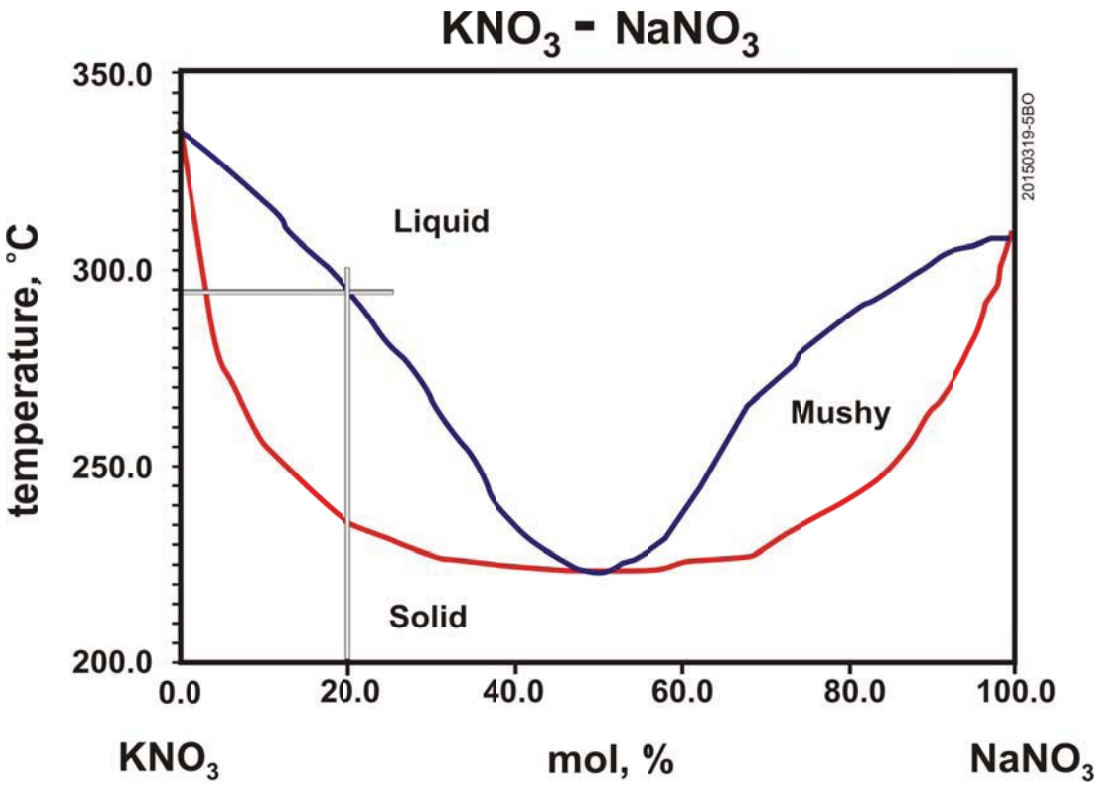

Figure 2. KNO_3- $NaNO_3$ phase diagram (regenerated based on Fluhrer et al. [9]).

3.2. MAAP Models Invoked:

Three major models in MAAP5 are exercised during the LIVE benchmarking. First, the lower plenum debris bed model is invoked via a call to subroutine DBBED. The debris bed is composed of a melt pool and surrounding crusts. The melt pool heats up by decay heat. It loses heat to the crusts by convection heat transfer. The crusts grow or shrink depending on the heat they received on the interface and conduction within the crusts.

- In MAAP4 and earlier versions of MAAP5, the lower plenum debris bed was represented as three homogeneous layers:
  - The top debris layer was the particle bed. The particle bed is assumed to remain on top as additional material is added to the debris bed. This model did not account for the possibility that particles could be submerged in the oxide pool.
  - The middle debris layer was the metal layer. All metal added to the debris bed was assumed to be molten and immediately added to this layer.
  - The bottom debris layer was the oxide pool. The oxide pool was modeled as a combination of a top crust, multiple bottom crusts, single embedded crust (on the CRD tubes when applicable) and a central molten region with uniform composition and temperature.

This approach assumes uniform composition of material within each of the three layers, and does not account for variations in composition of material, or the variation of temperature within the central molten region of the oxide pool, that would be expected in real systems.

- In MAAP 5.04 Alpha, the lower plenum debris bed model is refined:
  - The particle bed is nodalized into radial rings (consistent with core radial nodalization). This model accounts for the possibility that particles could be submerged in the molten corium.
  - The debris bed is treated as a mix of partially molten material including UO_2 and other oxides, and liquid metal, such as steel and zirconium. The liquid metal is less dense than the oxides, so it rises to the top, gradually forming a liquid metal layer which floats at the top of the debris.
  - The debris bed is represented as layers of differing composition and temperature. Hence, corium entering the lower plenum forms layers of differing temperature and composition.

This model represents the global circulation flow pattern in the molten corium pool (central region) in the lower plenum, which allows material flow between layers. The corium pool consists of three regions: an upper well-mixed isothermal region, a stably stratified lower region and a wall boundary layer (see Figure 3). The cold, descending boundary layer along the spherical wall generates an upward vertical flow in an otherwise stably stratified lower pool region. The relatively cold upper boundary of the pool produces a turbulent and well-mixed, nearly-isothermal upper-pool layer. An important byproduct of the model is the prediction of the vertical temperature distribution in the core of the pool. Particle bed, metal layer and embedded crust are not applicable to the particular problem presented in this paper.

Second, the conduction heat transfer model within the vessel wall is invoked. The vessel wall receives heat from the crust by conduction and loses heat to the cooling channel by convection. Twenty-five axial nodes are specified to model the lower head for the benchmark calculations.

Third, the insulation cooling channel is modeled in subroutine BLIVEB. Water is introduced into the insulation cooling channel at the bottom. The water heats up as it flows upward and receives heat from the vessel wall.

The radiation heat transfer on top of the crust to the uncovered vessel wall and reactor internals is considered in MAAP5. However, the calculation is superseded by the LIVE benchmark-specific

calculation in subroutine BLIVEB. Heat radiates from the melt top to the lid, and also to the uncovered part of the vessel wall. The lid radiates back to the uncovered part of the vessel wall. The lid is insulated outside.

4. RESULTS AND DISCUSSION

The lower plenum debris bed layering model is benchmarked against the LIVE experiments. The benchmarking is applicable for both LIVE-L1 and LIVE-L3 tests since these two tests are nearly identical except for the melt pour location. The results are compared against the steady state crust thickness, local heat flux and temperature measurements made during the 10 kW and 7 kW heating stages. Twenty-five axial nodes are used to model the vessel wall and crust.

The BALI correlation is used for the convective heat transfer coefficient in the melt pool. Unlike the prototypic corium pool in a reactor vessel, where about half the decay heat is removed upward and the other half downward, the LIVE test vessel had an insulated lid and only about 20% of heat generated in the melt pool was removed upward. The remaining 80% was removed downward. No upper crust was observed in the melt pool in LIVE experiments. The BALI correlation is dependent on the volumetric heat generation in the melt pool. Therefore, for a given volumetric heat generation, the non-prototypic pool of the LIVE experiments would have stronger natural convection current and higher heat transfer coefficients than predicted by the BALI correlation. Therefore, the downward heat transfer coefficient given by the BALI correlation is increased by a factor of 1.6 to account for the 60% higher downward heat loss in LIVE experiments compared to the prototypic corium pool for a given volumetric heat generation. The upward heat transfer coefficient is not changed.

The thermal conductivity of the crust is assumed to be 0.52 W/m-K, the average value measured at various locations in the crust. The heat inputs in the crust nodes are estimated using the measured crust thicknesses and the location of heater arrays.

Figure 4 and Figure 5 show the measured and predicted melt pool temperatures during the 10 kW and 7 kW heating stages. The pool temperatures predicted by MAAP5 are compared against the temperatures measured at three different heights in the melt pool. The measurements are in good agreement with the data. However, the calculations slightly under predict the measurements. This is attributed to the scheme that is being used to correct the Bali correlation for this particular application and the uncertainty in the measurements (not reported in Ref. [9]).

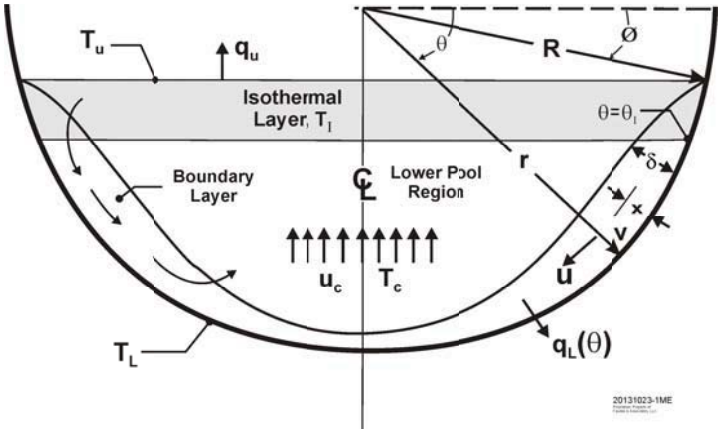

Figure 3. Corium pool convection model.

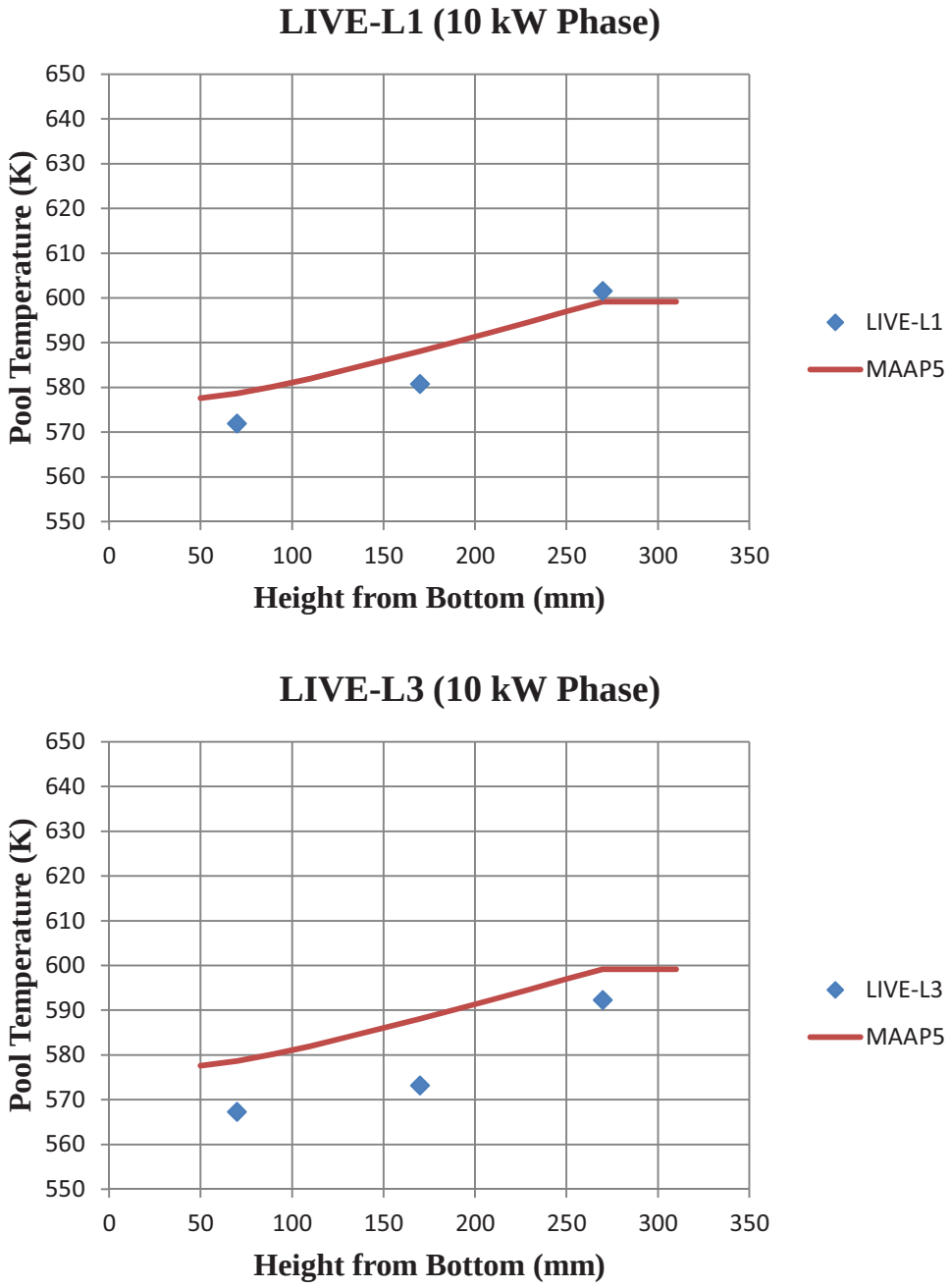

Figure 4 Comparison of measured and calculated pool temperature during 10 kW heating – measurements made 50 mm off the pool centerline.

The measured pool temperatures increase monotonically from the bottom to the top of the melt pool. This is an expected trend since the molten material rising in the center of the pool due to natural circulation heats up as it rises. The layering model, with the convecting pool model, is responsible for producing the axial temperature gradient in the melt pool.

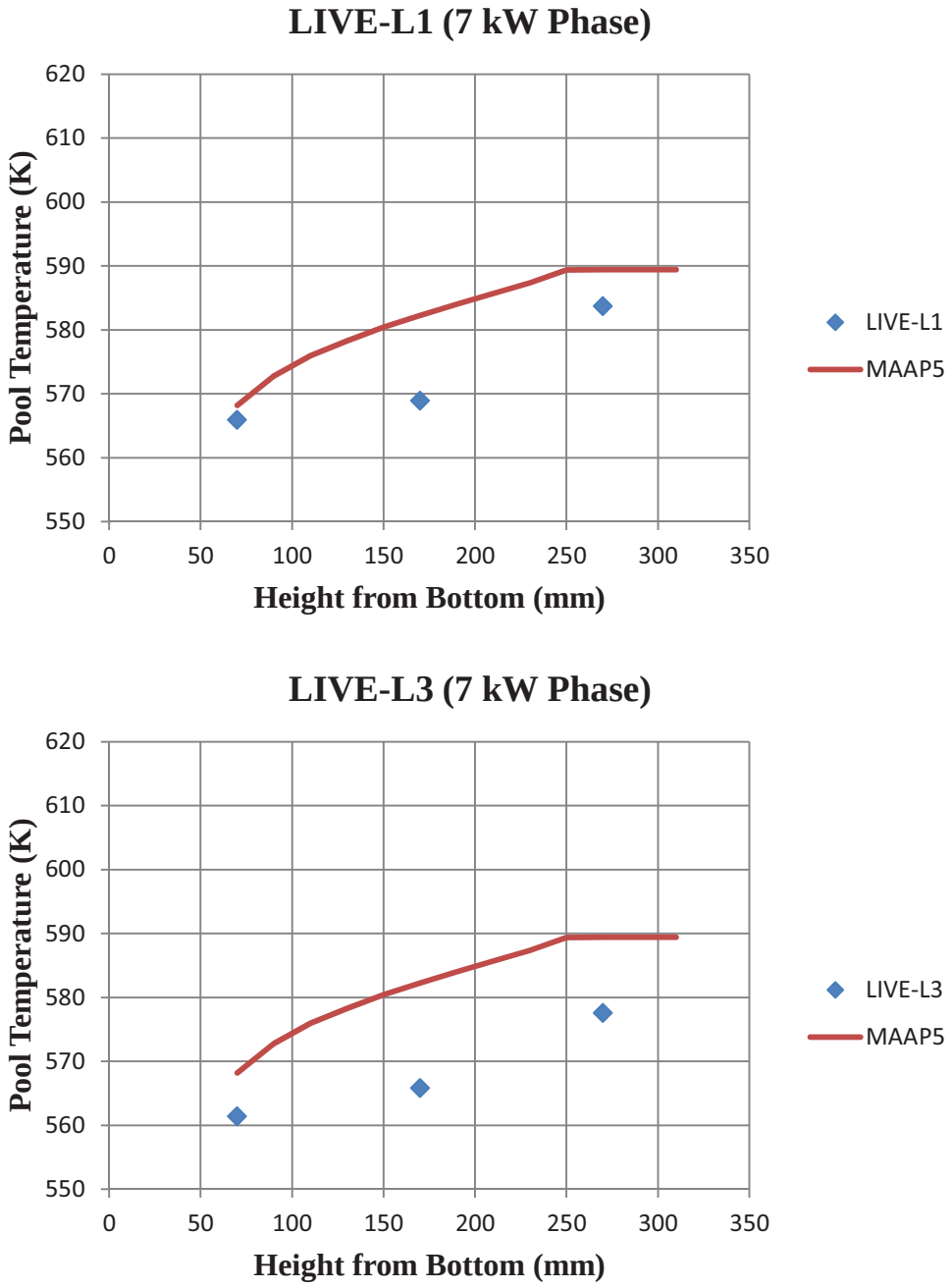

Figure 5 Comparison of measured and calculated pool temperature during 7 kW heating – measurements made 50 mm off the pool centerline.

Figure 6 and Figure 7 show the measured and predicted heat fluxes on the vessel wall. In general, the heat flux increases monotonically from the bottom to the top of the pool. LIVE test results show a decrease in heat flux between 0° and 30°, which is expected to be due to discrete heater array locations. The last measurement, which was

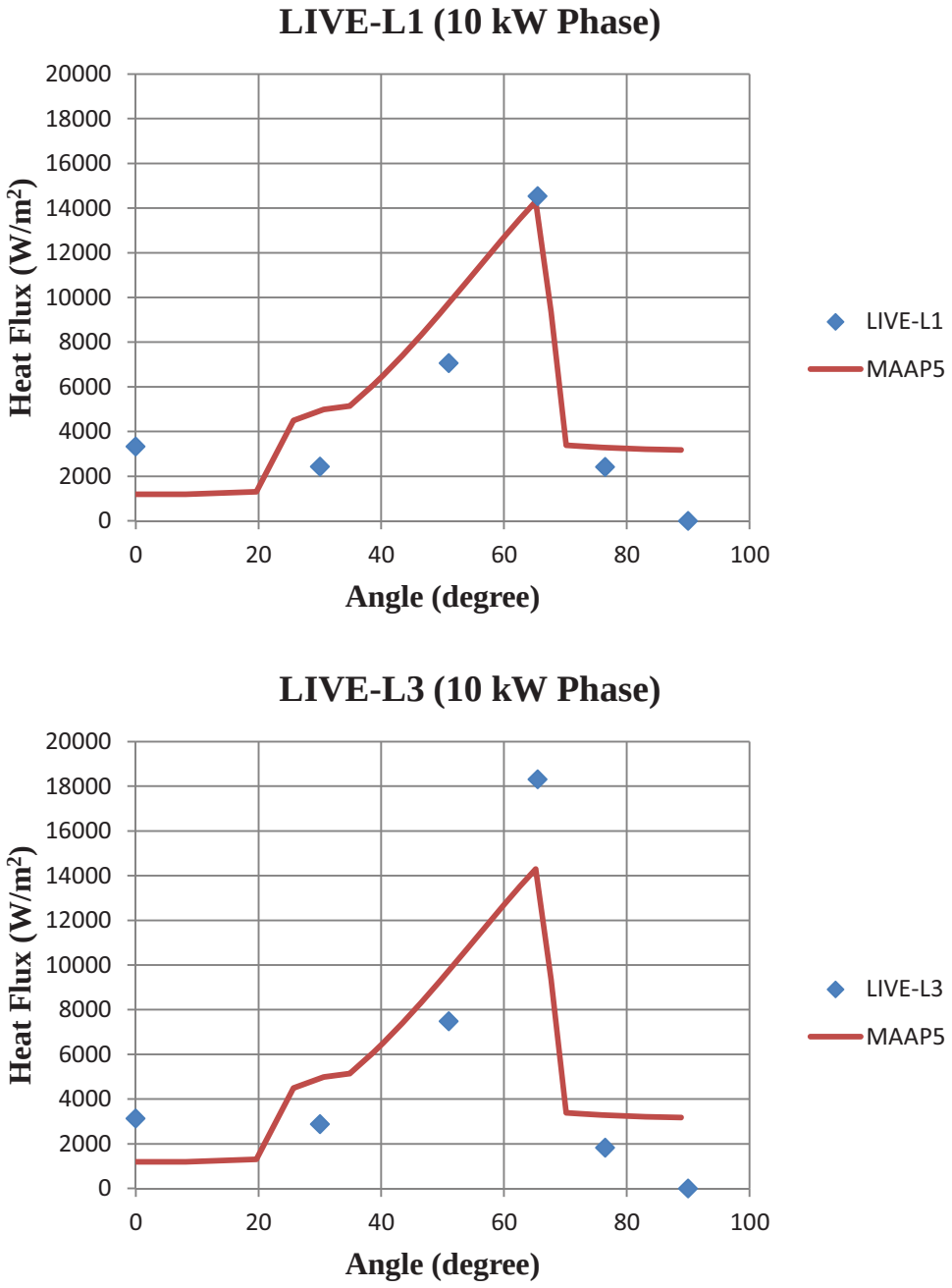

Figure 6 Comparison of measured and calculated heat flux during 10 kW heating.

made at 76.5°, is located outside of the pool. This location was not covered by the melt, but was receiving radiation heat from the pool surface. Therefore, the heat flux at this location was lower than at 65.5°. The comparisons of the measured and calculated heat flux values are in generally good agreement with each other. The uncertainty of the heat flux measurements is not reported by Ref. [9] but it should be due to combined uncertainties of the thermocouples on the vessel wall used for heat flux measurements.

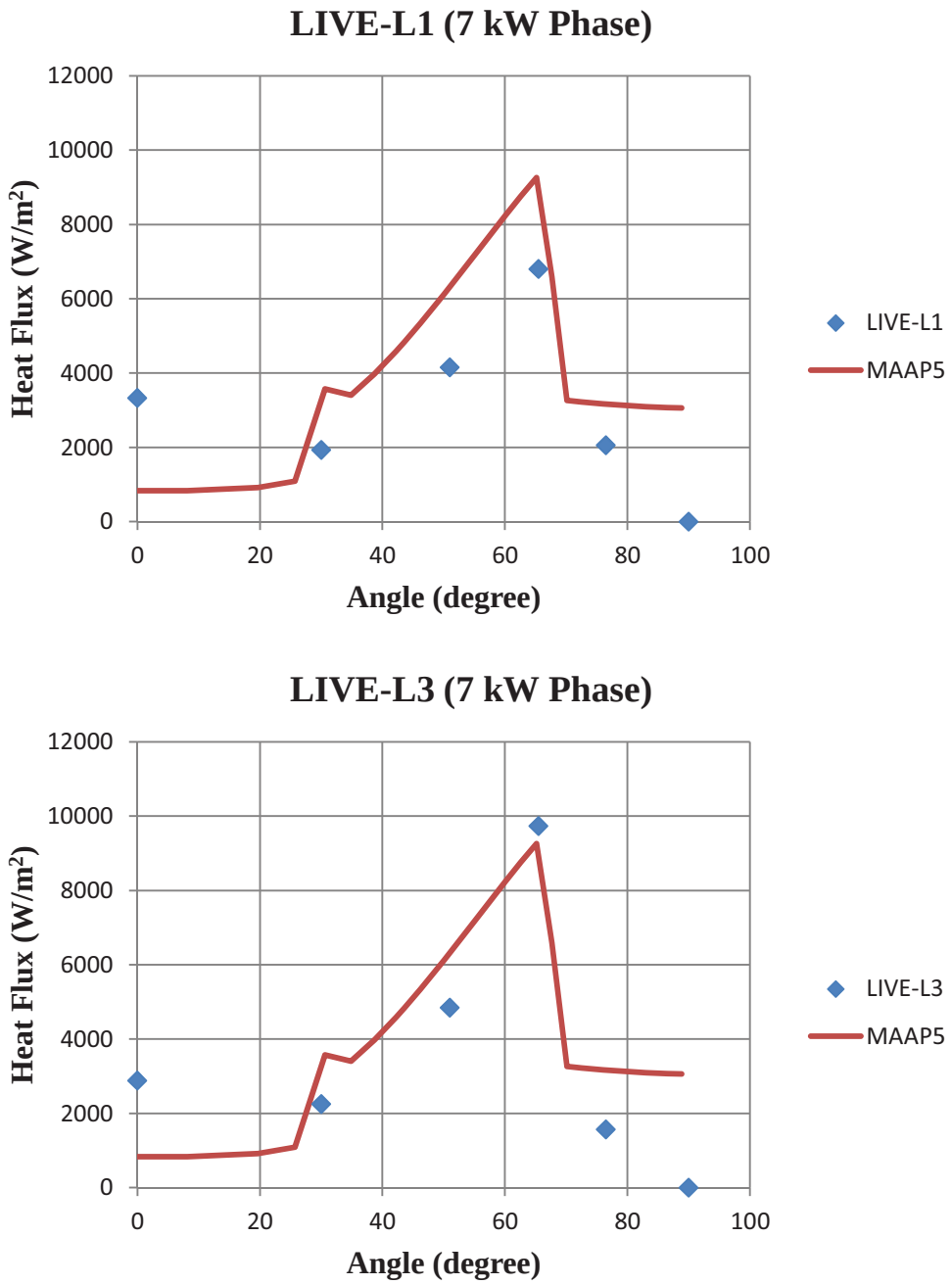

Figure 7 Comparison of measured and calculated heat flux during 7 kW heating.

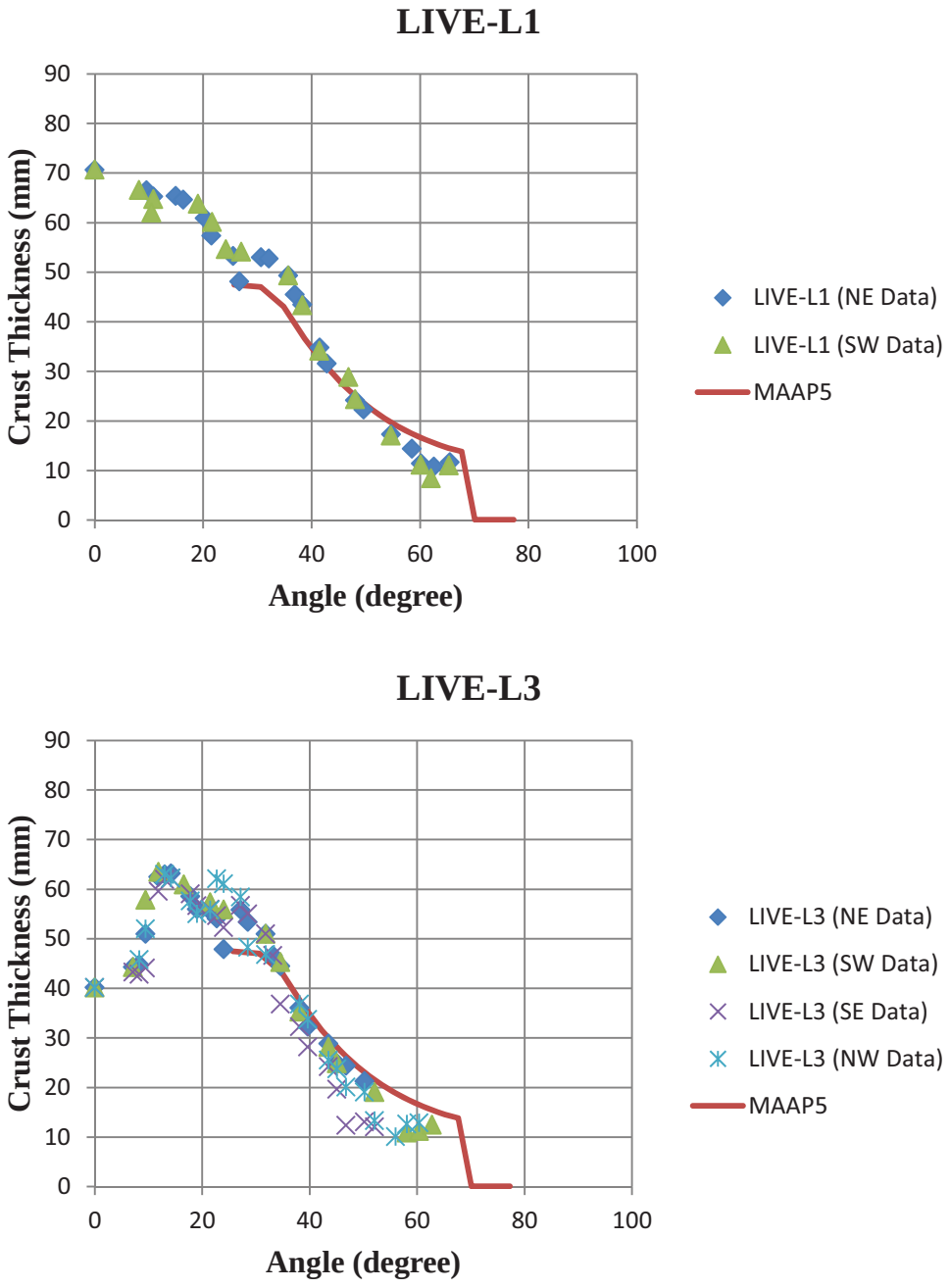

Figure 8 Comparison of measured and calculated crust thickness.

Figure 8 shows the measured and predicted crust thicknesses. Normally, the crust is thickest at the bottom and gradually gets thinner towards the top. In the LIVE-L3 test, the crust thickness had a local dip at the bottom due to the presence of the heater array in the crust (~40 mm from the bottom of the vessel). However, in the LIVE-L1 test the local dip in the bottom crust was missing. Based on an email communication with the investigator who conducted the LIVE tests, this difference was attributed to incomplete removal of molten material from the test apparatus at the end of the LIVE-L1 test, which subsequently formed an additional crust at the bottom of the vessel.

5. CONCLUSIONS

The lower plenum models related to molten pool behavior and crust formation in MAAP5 is benchmarked against the LIVE-L1 and LIVE-L3 test results. The experimental test facility and procedures are described. The key measured quantities are explained. The comparisons showed reasonably good agreement with the experimental data. The non-prototypic melt pool (no top crust) and discrete heating arrays are identified as important factors affecting the benchmarking.

ACKNOWLEDGMENTS

This work is sponsored under contracts from Atomic Energy of Canada Limited, Electric Power Research Institute (EPRI), Toshiba Corporation and Japanese Ministry of Economy.

REFERENCES

1. Kymalainen, O., Hongisto, O., Antman, J., Tuomisto, H. and Theophanous, T.G. (1992). COPO: Experiments for Heat Flux Distribution from a Volumetrically Heated Corium Pool, paper presented at the NRC Light Water Reactor Information Meeting.
2. Bonnet, J. M., and Seiler, J. M., 1999, "Thermal-Hydraulic Phenomena in Corium Pools for Ex-Vessel Situations: the BALI Experiment," Proceedings of the International Conference on Nuclear Engineering (ICONE 7), April 19-23, Tokyo, Japan.
3. Theofanous, T. G., Liu, C., Addition, S., Angelini, S., Kymalainen, O., Salmassi, T., 1996, "In-Vessel Coolability and Retention of a Core Melt," DOE/ID-10460, October 1996.
4. Gaus-Liu, X., Miassoedov, A., Cron, T., Wenz, T. (2010). In-vessel Melt Pool Coolability Test-Description and Results of LIVE Experiments, Nuclear Engineering and Design 240, 3898–3903.
5. Gauntt, R.O., et al. (2005), MELCOR Computer Code Manuals, NUREG/CR-6119, Vol. 2, Rev.3, Sandia National Laboratories, USA.
6. SCDAP/RELAP5-3D Code Development Team (2003). SCDAP/RELAP/MOD3D Code Manual, Volume II: Modeling of reactor core and vessel behavior during severe accidents, INEEL/EXT-02-00589, Rev. 2.2, INEEL, USA.
7. Van Dorsselaere, J.P., et al. (2009). The ASTEC Integral Code for Severe Accident Simulation, Nuclear Technology, 165, 293-307.
8. FAI, 2013, "Transmittal Document for MAAP Code Revision MAAP 5.02 Beta July 2013", Fauske and Associates, LLC Report No. FAI/13-0441.
9. Fluhrer, B., Miassoedov, A., Cron, T., Foit, J., Gaus-Liu, X., Schmidt-Stiefel, S., Wenz, T., Ivanov, I. and Popov, D. (2008). The LIVE-L1 and LIVE-L3 Experiments on Melt Behavior in RPV Lower Head, Institut für Kern- und Energietechnik Programm Nukleare Sicherheitsforschung, FZKA 7419.